GABA regulation of burst firing in hippocampal astrocyte neural circuit: A biophysical model

Junxiu Liu [1,*], **Liam McDaid** [1], **Alfonso Araque** [2], **John Wade** [1], **Jim Harkin** [1], **Shvan Karim** [1], **David C. Henshall** [3,4], **Niamh M. C. Connolly** [3], **Anju P. Johnson** [5], **Andy M. Tyrrell** [5], **Jon Timmis** [5], **Alan G. Millard** [5], **James Hilder** [5], **David M. Halliday** [5]

[1] *School of Computing, Engineering and Intelligent Systems, Ulster University, UK.*
[2] *Department of Neuroscience, University of Minnesota, Minneapolis, USA.*
[3] *Department of Physiology and Medical Physics, Royal College of Surgeons in Ireland, Dublin 2, Ireland.*
[4] *FutureNeuro Research Centre, RCSI, Dublin, Ireland*
[5] *Department of Electronic Engineering, University of York, York, UK.*

Correspondence*:
School of Computing, Engineering and Intelligent Systems, Ulster University, Magee campus, Northern Ireland, UK. BT48 7JL
j.liu1@ulster.ac.uk

ABSTRACT

It is now widely accepted that glia cells and gamma-aminobutyric acidergic (GABA) interneurons dynamically regulate synaptic transmission and neuronal activity in time and space. This paper presents a biophysical model that captures the interaction between an astrocyte cell, a GABA interneuron and pre/postsynaptic neurons. Specifically, GABA released from a GABA interneuron triggers in astrocytes the release of calcium (Ca^{2+}) from the endoplasmic reticulum via the inositol 1, 4, 5-trisphosphate (IP_3) pathway. This results in gliotransmission which elevates the presynaptic transmission probability rate (PR) causing weight potentiation and a gradual increase in postsynaptic neuronal firing, that eventually stabilises. However, by capturing the complex interactions between IP_3, generated from both GABA and the 2-arachidonyl glycerol (2-AG) pathway, and PR, this paper shows that this interaction not only gives rise to an initial weight potentiation phase but also this phase is followed by postsynaptic bursting behaviour. Moreover, the model will show that there is a presynaptic frequency range over which burst firing can occur. The proposed model offers a novel cellular level mechanism that may underpin both seizure-like activity and neuronal synchrony across different brain regions.

Keywords: astrocyte cell, GABA interneuron, burst firing, calcium oscillation, potentiation

1 INTRODUCTION

Spiking neural networks (SNNs) are considered to be the most biologically plausible representation of brain function (Ghosh-dastidar and Adeli, 2009). Additionally, SNNs capture a Hebbian type learning paradigm where the timing between pre and postsynaptic spikes dictates whether synaptic depression or

potentiation occurs (Song et al., 2000). SNNs have also been shown to be effective in time series prediction (Reid et al., 2014), spatiotemporal pattern recognition (Hu et al., 2013), and system control (Liu et al., 2015) in various application domains. In SNNs, the neurons and synapses are fundamental components in the network, where the information is encoded in spikes or action potentials for transmission between
25 neurons (Izhikevich, 2003). In the central nervous system neurons receive input stimuli and respond by firing spike patterns such as bursting, which has been observed in the hippocampus of rodents (Miles and Wong, 1986), electric fish (Gabbiani et al., 1996) and in the primary motor cortex, brainstem and thalamus within the somatomotor system of humans (Arichi et al., 2017). The bursts can, in some cases, represent normal brain function and in other cases abnormal brain function (e.g. epilepsy) (Halassa et al., 2007;
30 Araque et al., 1999).

Research has shown that astrocytes, one type of glial cell, modulate neuronal activity (Halassa et al., 2007; Breslin et al., 2018; Flanagan et al., 2018) where a single astrocyte may enwrap a large number of synapses ($\sim 10^5$ synapses), and connect to several neighbouring neurons (four-eight). The interplay between an astrocyte and the neighbouring neurons is believed to occur at the tripartite synapse (Araque
35 et al., 1999), which is bi-directional and serves, in some cases, to modulate the synaptic transmission probability rate (PR): via the direct/indirect retrograde signalling messenger endocannabinoids (Wade et al., 2012). This gives rise to re-modelling of the SNN connectivity (Naeem et al., 2015; Liu et al., 2018; Johnson et al., 2018; Wade et al., 2011).

It has also been reported that gamma-aminobutyric acidergic (GABA) interneurons participate in astrocyte-
40 mediated control of excitatory synaptic transmission (Perea et al., 2016) and exercises control over the firing frequency of pyramidal cells. Furthermore GABA release synchronises principal cell population discharge contributing to the generation of rhythmic activity in neuronal networks, such as theta and gamma frequency oscillations (Kullmann, 2011). A recent paper reported that GABA released in proximity to a tripartite synapse can activate GABA-B receptors on the astrocyte leading to gliotransmission, which is
45 known to regulate synaptic transmission probability (Liu et al., 2018). The research reported in (Kullmann, 2011; Liu et al., 2018; Kurosinski and Götz, 2002) provides the underpinning for the work presented here.

In this paper, we investigate the coupling between a GABA interneuron, an astrocyte terminal and the pre and postsynaptic terminals. The main contributions of this paper include (i) a novel biophysical model that describes the signalling pathways at the tripartite synapse and (ii) a novel mechanism that can potentially
50 explain postsynaptic neuron burst firing. The rest of paper is organized as follows. Section 2 presents the biophysical model while section 3 provides simulation results that demonstrate the bursting. Section 4 concludes the paper and discusses future work.

2   BIOPHYSICAL MODEL OF A NETWORK BURSTING

In this section, a detailed discussion of the signalling pathways at the tripartite synapse is presented with a specific focus on GABA signalling between the presynaptic terminal and the nearby astrocyte. It will be
55 shown that this interplay acts as a frequency dependent switch, which modulates the probability of release (PR) at the presynaptic terminal. Our Ca^{2+} dynamics model shows that calcium (Ca^{2+}) oscillations only occur over a range of inositol 1, 4, 5-trisphosphate (IP_3) concentrations and furthermore this paper will show that Ca^{2+} oscillations are periodic and this behaviour is key to the bursting behaviour.

2.1 Signalling pathways and activity regulations

60   The conventional tripartite synapse has three terminals: the presynaptic axon, postsynaptic dendrite and the astrocyte cell (Wade et al., 2012; Liu et al., 2018). In this paper we consider earlier work where, in a hippocampal astrocyte neural network, GABA interneurons interact with excitatory tripartite synapses to dynamically change the synaptic transmission behaviour from inhibitory to excitatory through modulation of PR (Perea et al., 2016). The signalling pathways between the GABA interneuron and tripartite synapse

65   are shown in Fig 1. When an input stimulus of frequency (f_{pre}) is present at the excitatory presynaptic axon, neurotransmitter (glutamate) is released into the cleft and subsequently binds to receptors at the postsynaptic dendrite causing the depolarization of the postsynaptic neuron. While the authors accept that fast-spiking interneurons can fire at much higher frequencies than glutamatergic neurons, in this work we assume for simplicity that the firing rate of the GABA interneuron (f_{GABA}) follows f_{pre}, as the most

70   likely physiological condition would be the activation of GABA interneuron by activation of glutamatergic axons (Serrano et al., 2006; Covelo and Araque, 2018). While GABA initially binds to GABA-A receptors inhibiting synaptic transmission and post-synaptic neuronal activity, recent work (Perea et al., 2016) has shown that with repeated firing of GABA interneurons, GABA also binds to GABA-B receptors on the astrocyte membrane, resulting in a switch from inhibition to excitation at the presynaptic terminal, and an

75   associated excitatory response at the postsynaptic terminal. In this paper we focus on astrocyte-mediated GABA-induced excitation since the postsynaptic inhibition was found negligible, and the transient acute presynaptic inhibition was overpowered by the astrocyte signalling during sustained activity (Perea et al., 2016). Hence, our model dos not incorporate these negligible or transient inhibitory effects, focusing in the sustained mechanisms and effects of inhibitory signalling through astrocyte activation.

80   As f_{GABA} increases, the GABA concentration level in the extracellular space increases, and a level is reached whereby binding to GABA-B receptors on the astrocyte membrane commences, leading to the production of IP_3: we subsequently refer to IP_3 due to GABA as IP_3^{GABA}, which contributes to the overall cytosolic IP_3 (Perea et al., 2016). IP_3^{GABA} is a secondary messenger which is degraded when released into the cytoplasm: initially cytosolic Ca^{2+} and IP_3 levels are low and therefore degradation

85   of IP_3 will also be low, as the degradation rate correlates with both Ca^{2+} and IP_3 concentrations. This degradation is gradually overcome with increasing levels of GABA and the $PLC\delta$ signalling pathway, which is modulated by Ca^{2+} and is accounted for in this work. Finally IP_3^{GABA} starts to bind to IP_3 receptors (IP_3R_s) on the Endoplasmic Reticulum (ER). When the total cytosolic IP_3 is sufficiently high, Ca^{2+} is released from the ER (De Pittà et al., 2009). At some point both IP_3 and Ca^{2+} reaches a level at

90   which an oscillating Calcium-Induced Calcium Release (CICR) occurs from the ER (Marchant et al., 1999): hereafter referred to as T_{CICR}. Several mechanisms are believed to contribute to Ca^{2+} oscillation but there is still much debate around this topic. For example, IP_3R_s have binding sites for both IP_3 and Ca^{2+}, and Ca^{2+} release from the ER is believed to rely on coincidence binding of these ions. The time between IP_3 and Ca^{2+} binding depends on the concentration of these ions and therefore this could explain why Ca^{2+}

95   is believed to be a regulator of IP_3R_s activity: at low Ca^{2+} levels IP_3R_s activity is increased, whereas the opposite is true at high Ca^{2+} levels. This is in agreement with other research (Dawson, 1997). However, there is not enough experimental evidence on these receptors to formulate a sufficiently detailed model. Therefore, in this work we revert to a hitherto accepted model (Perea et al., 2016) where Ca^{2+} oscillatory behaviour is believed to arise from the feedback interplay between Ca^{2+}, IP_3 and IP_3 degradation. As

100   Ca^{2+} and IP_3 rapidly increase there is a complex dependency between the concentrations of both Ca^{2+} and IP_3 and Ca^{2+}/IP_3-induced degradation of IP_3, which is the dominant process at elevated Ca^{2+}/IP_3 levels. Therefore, a transient elevation of Ca^{2+} and/or IP_3 is followed by a rapid drop in IP_3, which can

reduce IP_3 to below T_{CICR}. At this point degradation of IP_3 is weak because both the Ca^{2+} and IP_3 levels have fallen and therefore IP_3 starts to increase again due to IP_3^{GABA}. When the T_{CICR} level is reached again a transient elevation of Ca^{2+} re-occurs. We will demonstrate that our results support this behaviour. This oscillatory behaviour causes the release of the glutamate from the astrocyte (gliotransmitter) into the synapse (see Glu (e-SP) pathway in Fig 1), which binds to pre-synaptic group I metabotropic Glutamate Receptors (mGluRs) at the presynaptic terminal. This signalling pathway results in an increase in PR at the presynaptic terminal (Navarrete and Araque, 2010).

As PR increases more glutamate is released into the cleft and potentiation/depression of the synaptic weight can commence with the availability of glutamate to bind to N-methyl-D-aspartate (NMDA)-type glutamate receptors (Lüscher and Malenka, 2012). While we acknowledge that the biophysical mechanisms regulating the functional dependency between PR and plasticity are complex and not fully understood, we propose that PR acts as a "switch" which can turn on/off potentiation/depression at synaptic sites. To formulate a tractable mathematical model that captures this relationship we modulate the height of the Spike Timing Dependent Plasticity (STDP) associated plasticity window using PR: with $PR \geq PR^*$ (PR^* is defined as the plasticity activation level) the plasticity window fully opens and with $PR < PR^*$ the plasticity window closes. The decision on whether potentiation or depression occurs is governed by the STDP rule (Magee and Johnston, 1997) where potentiation occurs when the presynaptic spike precedes postsynaptic spike, otherwise depression occurs. Additionally, we consider the case where the
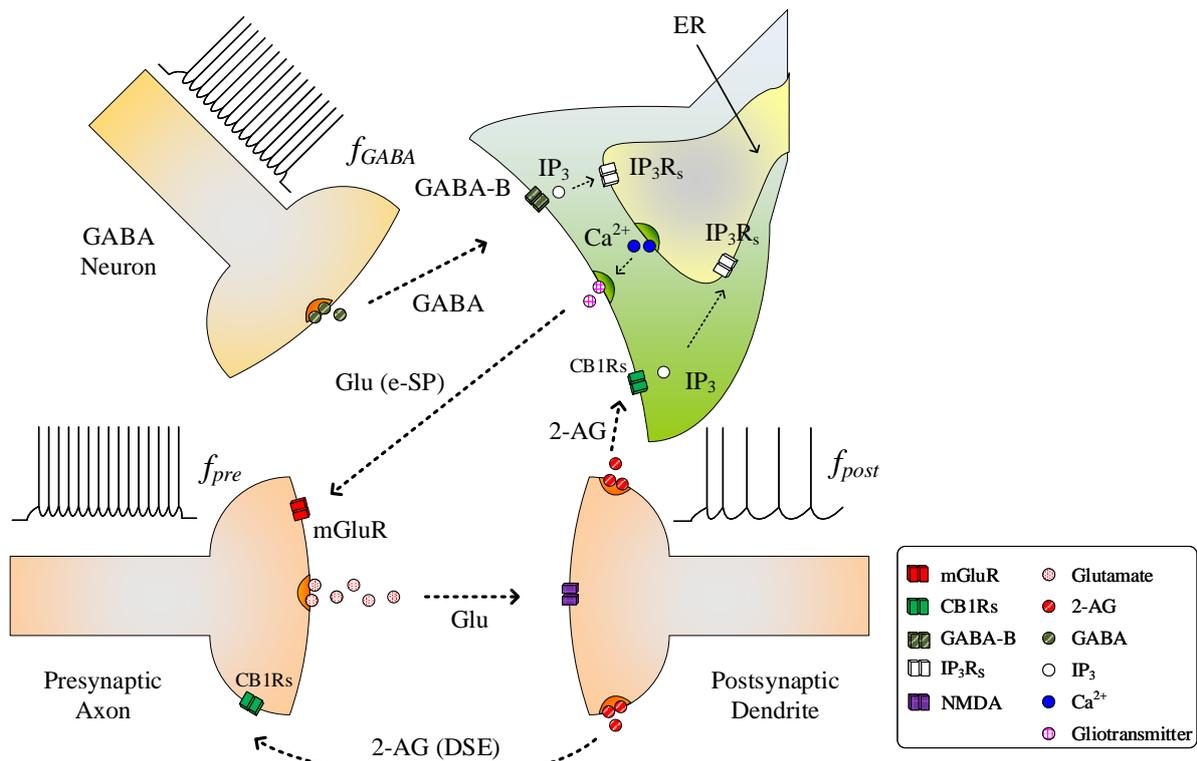
Figure 1. Signalling pathways at the tripartite synapse where GABA released from GABA interneuron binds to GABA-B receptors on the astrocyte membrane and IP_3^{GABA} is released into the astrocyte cytosol. 2-AG released from the postsynaptic neuron binds to the receptors on the astrocyte membrane triggering the generation of IP_3^{AG}. With f_{post} low and IP_3 reached a level, IP_3 induces Ca^{2+} release from the ER and gliotransmitter is released into the synaptic cleft (Glu (e-SP) pathway) where it binds to mGluR receptors on the presynaptic membrane. This causes an increase in PR and the plasticity window opens.
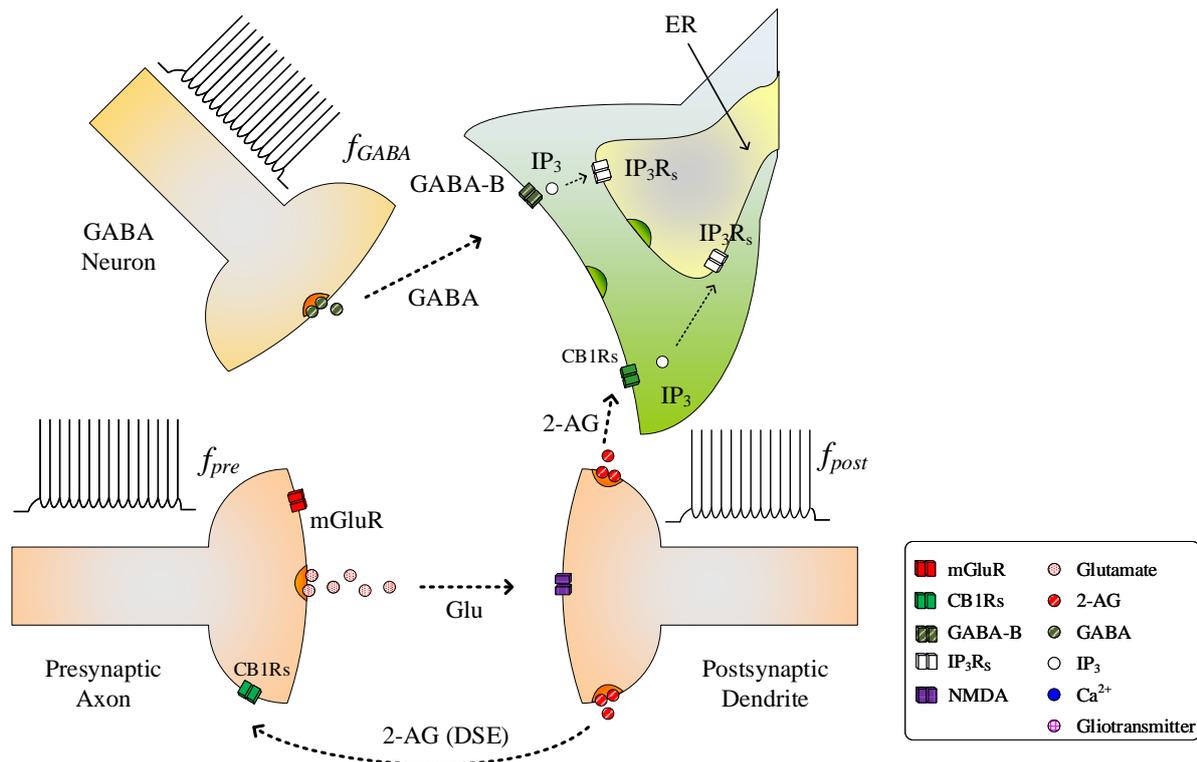
Figure 2. Signalling pathways of the tripartite synapse where for high f_{post} T_{CICR} is reached and hence the Ca^{2+} oscillation and the Glu (e-SP) pathway ceases causing PR to fall and the plasticity window shuts: PR also falls due to the increase in the 2-AG (DSE) pathway. Under this condition the level of neurotransmitter in the cleft falls to baseline and f_{post} diminishes.

postsynaptic neuron is sufficiently depolarized such that the retrograde messenger 2-arachidonyl glycerol (2-AG) is released from the postsynaptic neuron. Since the contribution of 2-AG signalling to the observed GABA-mediated regulatory effects of astrocytes on excitatory transmission is negligible (Perea et al., 2016), the authors take the view that 2-AG signalling onto GABAergic terminals would not be a significant factor
125 in network bursting. However, we do consider 2-AG binding to type 1 Cannabinoid Receptors (CB1Rs) on the astrocyte membrane which then initiates the release of the IP_3 into the cytoplasm of the astrocyte: we denote this secondary messenger as IP_3^{AG}.

During the synapse learning phase, the frequency of the postsynaptic neuron, f_{post}, is increasing, as is the 2-AG signal and consequently IP_3^{AG}. As IP_3^{AG} contributes to the total IP_3, IP_3 will eventually reach
130 a level where degradation of IP_3 no longer reduces IP_3 (and therefore Ca^{2+}) to below T_{CICR}. In this instance, both the oscillatory Ca^{2+} transient and Glu (e-SP) pathways cease (Liu et al., 2018), see Fig 2. In addition, the released 2-AG also binds to CB1Rs on the presynaptic terminal triggering the Suppression of Excitation (DSE) pathway, and results in a decrease in PR (Alger, 2002). Due to the reduction in the Glu (e-SP) pathway and the increase in the DSE pathway, PR decreases at the presynaptic terminal, the level of
135 neurotransmitter in the cleft then falls to baseline and the frequency of the postsynaptic f_{post} diminishes which in turn causes IP_3^{AG} to reduce. Furthermore, the total IP_3 degrades due to cytosolic degradation pathways including IP_3 3-kinase IP_3^{3K}, and dephosphorylation by inositol polyphosphate 5-phosphatase (IP_3^{5P}) (see Eq (11)). Together, these processes reduce IP_3 levels below T_{CICR}, and the rate of degradation diminishes sufficiently to allow IP_3 to increase again due to IP_3^{GABA}. When the T_{CICR} level is again
140 exceeded, Ca^{2+} oscillations re-commence, the Glu (e-SP) pathway is re-established, PR increases and the

level of neurotransmitter in the cleft is raised. In this post-learning phase PR cannot be elevated to a level where the plasticity window opens ($PR < PR^*$), as the postsynaptic neuron is active and therefore the 2-AG pathway leads to a reduction in PR due to the DSE pathway. Consequently, the postsynaptic neuron firing rate reaches a maximum when the T_{CICR} level is reached but it subsequently falls afterwards: a postsynaptic burst has occurred. This is followed by repeated bursts at each Ca^{2+} oscillatory period. We therefore propose that neuronal burst firing directly correlates with astrocytic Ca^{2+} oscillation.

Moreover, it should be noted that the duration of the burst correlated with the frequency of presynaptic terminal f_{pre} at the excitatory presynaptic axon. As f_{pre} increases so does the rate of increase of IP_3 and the burst period is reduced. Therefore, network bursting is f_{pre} dependant and will only occur over a range of f_{pre}.

2.2 Postsynaptic neuron model

In this paper, the Leaky Integrate and Fire (LIF) model (Gerstner and Kistler, 2002) is used due to the relatively low computing requirement and minimal parameters tuning. The LIF model is given by

$$\tau_m \frac{dv}{dt} = -v(t) + R_m \sum_{i=1}^{n} I_{syn}^i(t), \tag{1}$$

where τ_m is the neuron membrane time constant, v is the neuron membrane potential, R_m is the membrane resistance, I_{syn}^i is the current injected to the neuron membrane by i^{th} synapse, and n is the total number of synapses associated with the neuron. When the neuron membrane potential v is greater than the firing threshold value, v_{th}, the neuron fires and outputs a spike followed by a reset state or a refractory period ($\sim 2ms$). The release of 2-AG correlates with the postsynaptic neuron activity (Naeem et al., 2015) and this is expressed as

$$\frac{d(AG)}{dt} = \frac{-AG}{\tau_{AG}} + r_{AG}\delta(t - t_{sp}), \tag{2}$$

where AG denotes the released amount of 2-AG, τ_{AG} and r_{AG} are the 2-AG decay and production rates, and t_{sp} is the postsynaptic spike time. The released 2-AG binds to the CB1Rs at the presynaptic terminal and at the astrocyte terminal, and this will be discussed in Section 2.4.

2.3 GABA interneuron

The spike train at the presynaptic axon also presents at the GABA interneuron causing the release of GABA neurotransmitter (Perea et al., 2016), which can be described by

$$\frac{d(GABA)}{dt} = \frac{-GABA}{\tau_{GABA}} + r_{GABA}\delta(t - t_{sp}), \tag{3}$$

where GABA denotes the released amount of the neurotransmitter GABA, τ_{GABA} and r_{GABA} are the GABA decay and production rates, and t_{sp} is the presynaptic spike arrival time. GABA binds to the GABA-B receptors at the astrocyte cell and this is modelled in the next subsection.

2.4 Astrocyte cell

When GABA binds to GABA-B receptors on the astrocyte membrane, the amount of IP_3 released is given by

$$\frac{d(IP_3^{GABA})}{dt} = \frac{IP_3^{GABA*} - IP_3^{GABA}}{\tau_{ip3}^{GABA}} + r_{ip3}^{GABA}GABA, \tag{4}$$

where IP_3^{GABA} is the quantity of IP_3 generated by GABA within the cytoplasm, IP_3^{GABA*} is the baseline GABA level, τ_{ip3}^{GABA} is the decay rate of IP_3^{GABA} and r_{ip3}^{GABA} is the production rate of IP_3^{GABA}. When the postsynaptic neuron fires, the released 2-AG can also trigger IP_3 generation (Wade et al., 2012) and this is modelled by

$$\frac{d(IP_3^{AG})}{dt} = \frac{IP_3^{AG*} - IP_3^{AG}}{\tau_{ip3}^{AG}} + r_{ip3}^{AG}AG, \tag{5}$$

where IP_3^{AG} is the quantity of IP_3 generated by 2-AG within the cytoplasm, IP_3^{AG*} is the baseline level, τ_{ip3}^{AG} is decay rate of IP_3^{AG}, and r_{ip3}^{AG} is production rate of IP_3^{AG}.

In addition, the IP_3 production is also increased by the hydrolysis of the highly phosphorylated membrane lipid phosphatidylinositol $4, 5 - $ bisphosphate (PIP_2), such as the phosphoinositide-specific phospholipase C (PLC) isoenzyme of $PLC\delta$ (De Pittà et al., 2009). The $PLC\delta$ signalling is agonist independent and modulated by Ca^{2+} (De Pittà et al., 2009), and its activation rate can be modelled by

$$PLC\delta = PLC\delta' Hill(Ca^{2+}, K_{PLC\delta}, 2), \tag{6}$$

where the maximum $PLC\delta$-dependant IP_3 production rate (De Pittà et al., 2009) can be modelled by

$$PLC\delta' = \overline{PLC\delta'}/(1 + IP_3/K_\delta), \tag{7}$$

and K_δ is the inhibition constant of $PLC\delta$ activity. The Hill function (De Pittà et al., 2009) is described by

$$Hill(x, K, n) \equiv \frac{x^n}{x^n + K^n}, \tag{8}$$

where n is the Hill coefficient and K is the midpoint of the Hill function, namely the value of x at which $Hill(x, K, n)|_{x=K} = 1/2$.

The degradation of IP_3 mainly occurs through phosphorylation into inositol $1, 3, 4, 5$-–tetrakisphosphate (IP_4), catalysed by IP_3 3-kinase (3K), and dephosphorylation by inositol polyphosphate 5-phosphatase (5P). The rate of IP_3 degradation by IP_3^{5P} (De Pittà et al., 2009) can be modelled by

$$IP_3^{5P} \approx \overline{r}_{5P}IP_3, \tag{9}$$

where $\overline{r}_{5P}$ is the IP_3 degradation rate by IP-5P. The activity of IP_3^{3K} is regulated by Ca^{2+} in a complex fashion (De Pittà et al., 2009). The rate of IP_3 degradation by IP_3^{3K} can be modelled by

$$IP_3^{3K} = \overline{v}_{3K}Hill(Ca^{2+}, K_D, 4)Hill(IP_3, K_3, 1), \tag{10}$$

where $\overline{v}_{3K}$ is the maximum degradation rate by IP_3^{3K}, K_D is the Ca^{2+} affinity of IP_3^{3K}, and K_3 is the IP_3 affinity of IP_3^{3K}. Based on the previous contributions of IP_3, the total IP_3 is given by

$$IP_3 = IP_3^{GABA} + IP_3^{AG} + PLC\delta - IP_3^{5P} - IP_3^{3K}. \tag{11}$$

The Li-Rinzel model (Li and Rinzel, 1994) is used to model the Ca^{2+} dynamics within the astrocyte cell. The model consists of three channels, J_{chan}, J_{leak} and J_{pump}, where J_{chan} models the Ca^{2+} channel opening based on the mutual gating of the Ca^{2+} and IP_3, J_{leak} models the Ca^{2+} leakage from the ER into the cytoplasm and J_{pump} models how Ca^{2+} is pumped out from the cytoplasm into the ER via Sarco-Endoplasmic-Reticulum Ca^{2+}-ATPase (SERCA) pumps. The Ca^{2+} model in the approach of (De Pittà et al., 2009) is used in this work, and it is described by

$$\frac{d(Ca^{2+})}{dt} = J_{chan}(Ca^{2+}, h, IP_3) + J_{leak}(Ca^{2+}) - J_{pump}(Ca^{2+}), \tag{12}$$

$$\frac{dh}{dt} = \frac{h_\infty - h}{\tau_h}, \tag{13}$$

where J_{chan} is Ca^{2+} release depending on the Ca^{2+} and IP_3 concentrations, J_{pump} is the amount of stored Ca^{2+} within the ER via the SERCA pumps, J_{leak} is the Ca^{2+} leaking out of the ER and h is the fraction of activated IP_3R_s. The parameters h_∞ and τ_h are given by

$$h_\infty = \frac{Q_2}{Q_2 + Ca^{2+}}, \tag{14}$$

$$\tau_h = \frac{1}{a_2(Q_2 + Ca^{2+})}, \tag{15}$$

where

$$Q_2 = d_2 \frac{IP_3 + d_1}{IP_3 + d_3}. \tag{16}$$

J_{chan} is given by

$$J_{chan} = r_C m_\infty^3 n_\infty^3 h^3 (C_0 - (1 + C_1)Ca^{2+}), \tag{17}$$

where r_C is the maximal Calcium-Induced Calcium Release (CICR) rate, C_0 is the total free Ca^{2+} cytosolic concentration, C_1 is the ER/cytoplasm volume ratio, and m_∞ and n_∞ are the IP_3 Induced Calcium Release (IICR) and CICR channels respectively, which are given by

$$m_\infty = \frac{IP_3}{IP_3 + d_1}, \tag{18}$$

and

$$n_\infty = \frac{Ca^{2+}}{Ca^{2+} + d_5}. \tag{19}$$

J_{leak} and J_{pump} are described by

$$J_{leak} = r_L(C_0 - (1 + C_1)Ca^{2+}),$$ (20)

and

$$J_{pump} = v_{ER}\frac{(Ca^{2+})^2}{k_{ER}^2 + (Ca^{2+})^2},$$ (21)

where r_L is the Ca^{2+} leakage rate, v_{ER} is the maximum SERCA pump uptake rate and k_{ER} is the SERCA pump activation constant.

The intracellular astrocytic calcium dynamics are used to regulate the release of glutamate from the astrocyte: the Glu pathway. To model this release, it is assumed that when Ca^{2+} crosses the CICR threshold, a quantity of glutamate is released (Wade et al., 2012). It is described by

$$\frac{d(Glu)}{dt} = \frac{-Glu}{\tau_{Glu}} + r_{Glu}\delta(t - t_{Ca}),$$ (22)

where Glu is the quantity of released glutamate, τ_{Glu} is decay rate of glutamate, r_{Glu} is production rate of glutamate, and t_{Ca} is the time at which Ca^{2+} crosses the threshold. The released glutamate drives the generation of e-SP (Wade et al., 2012). The level of e-SP is modelled by

$$\tau_{eSP}\frac{d(eSP)}{dt} = -Glu + m_{eSP}Glu(t),$$ (23)

where τ_{eSP} is the decay rate of Glu, and m_{eSP} is a constant weight used to control the height of e-SP. It shows that the e-SP level depends on the glutamate released from the astrocyte cell.

The model of DSE in the approach of (Wade et al., 2012) is used to describe the relationship between the DSE and the released 2-AG from postsynaptic neuron. The DSE is assumed to change linearly with the cytosolic concentration of 2-AG, which is described by

$$DSE = AG \times K_{AG},$$ (24)

where AG is the concentration of 2-AG and K_{AG} is the scaling factor for the DSE.

2.5 Synapse model

For the synapse, a probabilistic model is employed which is based on the failure and success mechanisms of synaptic neurotransmitter release (Wade et al., 2012; Navarrete and Araque, 2010). A uniformly distributed pseudo-random number generator is used. If the generated random number $rand$ is less than or equal to the PR, a current I_{inj} is injected into the neuron which is shown by

$$I_{syn}^i(t) = \begin{cases} r_I * w_{syn}^i(t), & rand \leq PR \\ 0, & rand > PR \end{cases}$$ (25)

where r_I is the current production rate, and w_{syn}^i is the weight of the ith synapse. The associated PR of each synapse is determined by the DSE and e-SP together, which is given by

$$PR(t) = PR(t_0) + DSE(t)/100 + eSP(t)/100,$$ (26)

where $PR(t_0)$ is the initial PR for each synapse. As discussed in Section 2.1, the PR can switch on/off learning at the synaptic terminal by modulating the height of the plasticity learning window. The authors are not aware of any biophysical model that relates PR to the plasticity window weighting parameter A_0 and therefore in this work it is assumed that A_0 is modulated according to

$$A_0 = \begin{cases} 0, & PR \le PR^* \\ (PR - PR^*) * r, & PR > PR^* \end{cases} \qquad (27)$$

where PR^* is the learning activation level and r is a constant value which controls the maximum height of the learning window. The STDP rule used in this approach to update the synaptic weights according to the timing difference between the post and presynaptic spikes is described by

$$\delta w(\Delta t) = \begin{cases} -A_0 exp(\dfrac{\Delta t}{\tau_+}), & \Delta t \le 0 \\ A_0 exp(\dfrac{-\Delta t}{\tau_-}), & \Delta t > 0 \end{cases} \qquad (28)$$

where $\delta w(\Delta t)$ is the weight update, Δt is the time difference between the post and presynaptic spikes, A_0 is the height of the plasticity window which limits the maximum levels of weight potentiation and depression, and τ_+ and τ_- control the width of the plasticity window. A symmetrical plasticity window is assumed in this approach, and $\tau_+ = \tau_- = 40ms$.

From the proposed models, it can be seen that if the f_{pre} is large enough, IP_3 is generated sufficiently to cause Ca^{2+} oscillations. Then the Ca^{2+}-induced glutamate binds to the mGluRs receptors at the presynaptic terminal resulting in an increase of the synaptic transmission probability PR. Note that the authors wish to point out that astrocytes are believed to gate LTP and LTD by regulating glutamate levels in the synaptic cleft (Foncelle et al., 2018). Since there are many complex biophysical mechanisms involved in the regulation of glutamate, which are still under debate, the authors take the view that modulating the STDP plasticity window using PR is an effective way to capture this gating function. Elevating PR opens the synaptic plasticity learning window and over time f_{post} gradually increases which, via the 2-AG pathway, contributes to astrocytic IP_3 level until the Ca^{2+} oscillation stops. This is accompanied by a reduction in the Glu (e-SP) pathway and PR falls causing a reduction in f_{post}. Therefore, the bursting activity of the postsynaptic neuron is regulated by the GABA interneuron and the astrocyte cell. The results in the next section show the signalling pathways leading to a bursting postsynaptic neuron.

3 RESULTS

This section provides simulation results which highlight the dynamic behaviour at the synapse terminals and how the interactions between an astrocyte and GABA interneuron can give rise to bursting behaviour. The MATLAB simulation platform is used in this work together with the Euler method with the time step of 1 ms. Table 2 and Table 1 in the appendix give all the model parameters.

3.1 Bursting output spike pattern

In this simulation both the presynaptic excitatory neuron and the GABA interneuron are stimulated by the same spike train at frequency $f_{pre} = f_{GABA}$ which causes the release of GABA and glutamate (Perea et al., 2016). The presynaptic excitatory neuron/GABA interneuron stimulus is 40 Hz in the following simulations

as this is sufficient to produce a cytosolic $[IP_3] > 0.5\mu M$. With $PR > PR^*$ (see Fig 3), a significant increase occurs in the level of neurotransmitter in the cleft, the learning window opens (Fig 4) and weight potentiation starts (Fig 5) resulting in postsynaptic firing. Note that in Fig 4 the plasticity window height
265   parameter A_0 increases periodically with a corresponding potentiation of the synaptic weight (Fig 5). In our model the resting level for PR is 0.1 and based on the model in Eq (27), if $PR > PR^*$ ($PR^* = 0.45$ in this work), the STDP learning window opens ($A_0 > 0$) at ∼80 seconds, as shown in Fig 4. After the synaptic weight is potentiated, the synapse generates a depolarising current only when the input stimulus is presented at the presynaptic terminal and the PR value is greater than the value of a random number
270   (see probabilistic-based synapse model in equation Eq (25)): this current is injected into the postsynaptic LIF neuron. This injected current increases the postsynaptic potential and the neuron fires a spike if the membrane potential is greater than the firing threshold, v_{th}.
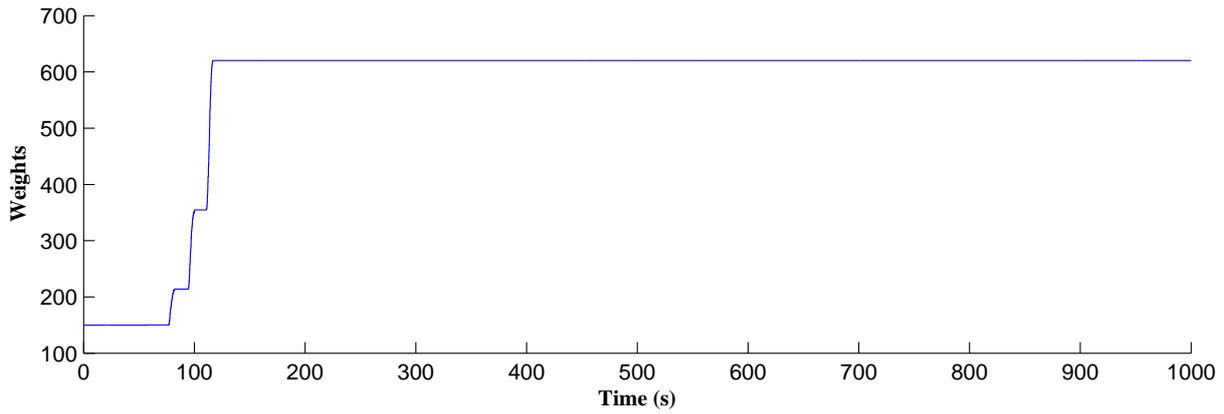
After a period of learning the postsynaptic neuron activity has stabilised and PR drops sufficiently, towards the end of the first set of PR "spikes" (see Fig 3), closing the plasticity window ($A_0 = 0$) and the
275   weight stabilises to ∼610 at 110 seconds, as shown in Fig 5: note that because the postsynaptic neuron is now active, $PR < PR^*$ for all subsequent Ca^{2+} oscillations as the DSE pathway is also active. Fig 6 shows the amount of GABA released by the GABA interneuron as a function of time where, as expected, GABA increases gradually and then stabilizes at 0.027 μM under the input spike stimulus. IP_3^{GABA} is
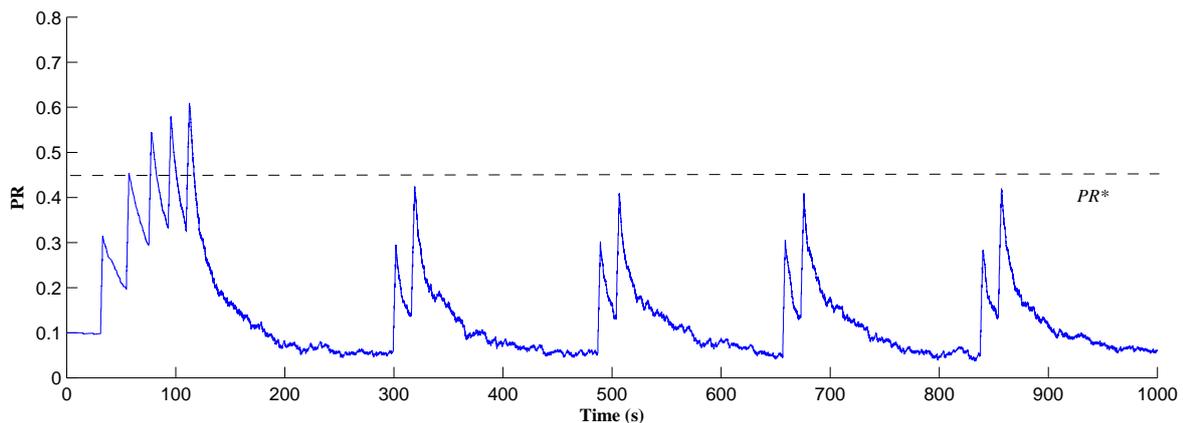

Figure 3. PR as a function of Glu (e-SP) and DSE signals over time. Note that the plasticity window will only be open when $PR > PR^*$ and this can be observed in Fig 4.
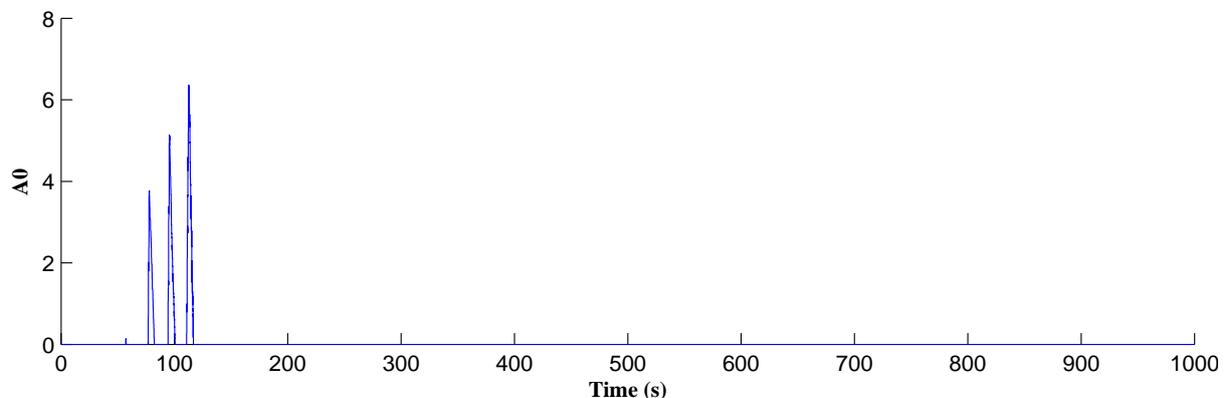

Figure 4. Plasticity window height A_0 as a function of time. Note that PR acts as a switch to open/close the plasticity window controlling the learning period.

Figure 5. Time dependant synaptic weight update governed by the STDP learning rule. When the plasticity window is open, learning commences, the synaptic weight begins to potentiate and after a period of learning the window shuts off and the synaptic weight stabilises.
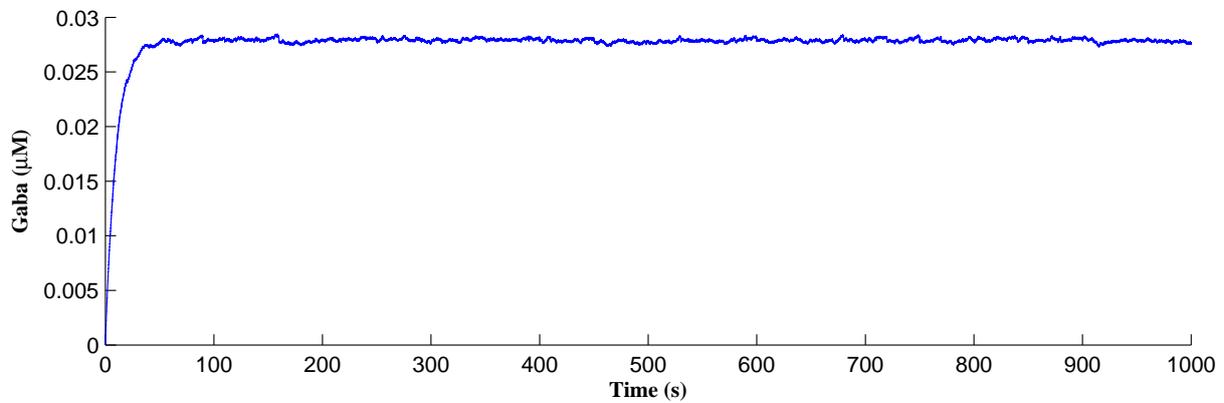

Figure 6. GABA released from the GABA interneuron as a function of time. Under the input spike stimulus of f_{GABA}, GABA increases and then stabilized.
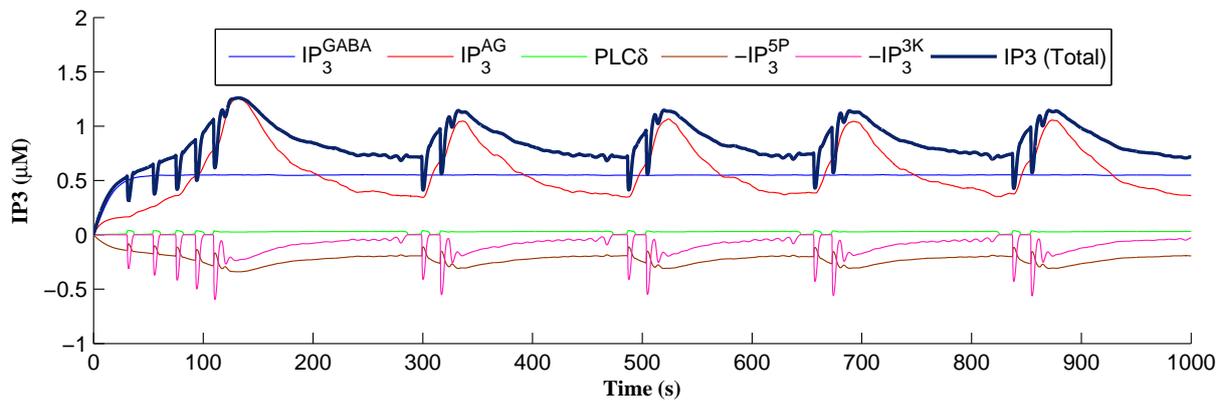

Figure 7. IP_3 dynamics within the astrocyte cell over time. The overall IP_3 includes contributions from IP_3^{GABA}, IP_3^{AG}, $PLC\delta$, IP_3^{5P} and IP_3^{3K}, where the degradations of IP_3, IP_3^{5P} and IP_3^{3K}, are shown as negative values.

shown in Fig 7 (blue) as a function of time and stabilizes at $\sim 0.58\mu M$ which is consistent with the input stimuli profile. Fig 7 shows the other IP_3 sources that contribute to the total IP_3 in the cytosol.

Initially the total IP_3 increases with IP_3^{GABA} until the T_{CICR} level is reached triggering the release of Ca^{2+}, as shown in Fig 8. We have observed from our model that T_{CICR} is consistent with an IP_3 level of
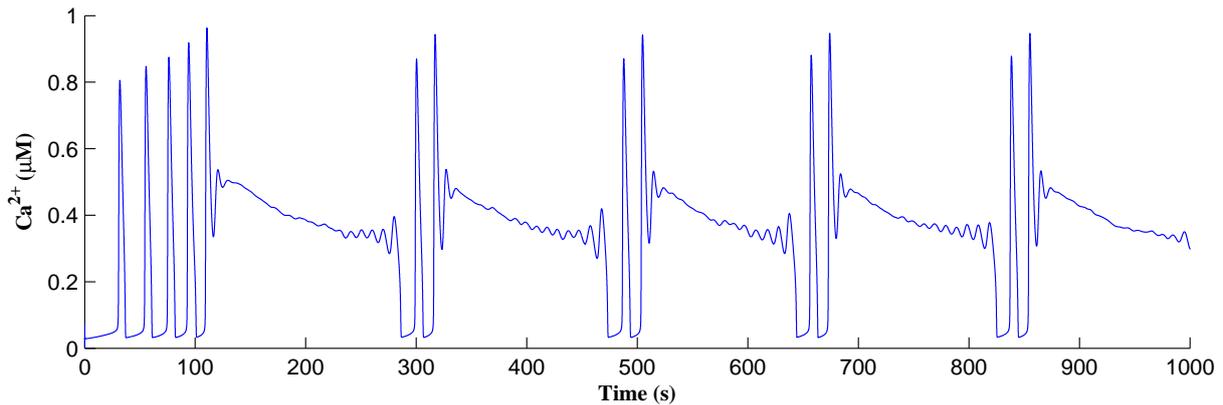
Figure 8. Ca^{2+} oscillations in the astrocyte cell as a function of time. Note a longer oscillatory period at the start due to learning but thereafter the oscillator period stabilises with constant on/off ratio.
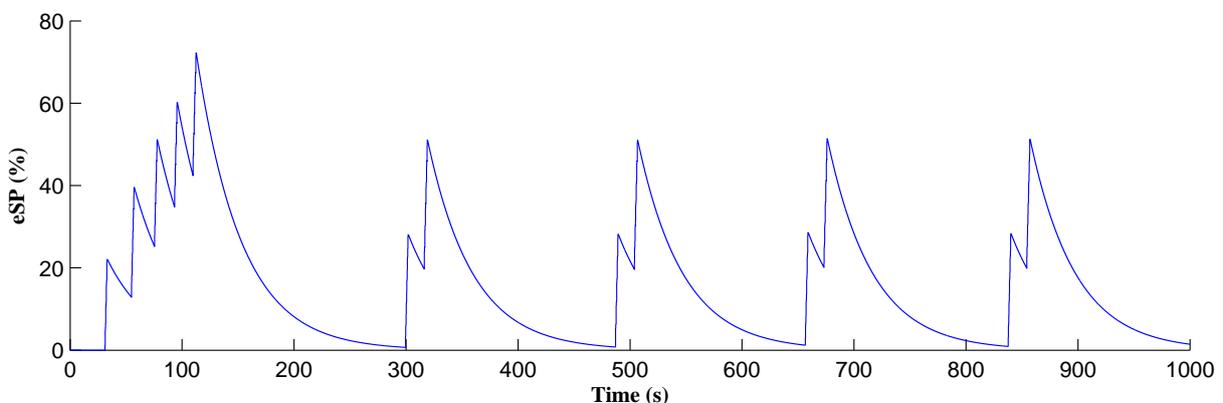

Figure 9. Glu (e-SP) signalling pathway as a function of time. Note a longer period of elevation of Glu (e-SP) at the start due to synaptic potentiation but thereafter the Glu (e-SP) profile repeats in time.

approximately 0.5 μM and whenever IP_3 exceeds this threshold a transient elevation in Ca^{2+} occurs, as can be seen in Fig 8. Note however that as the IP_3 level increases with IP_3^{AG} the degradation in IP_3 due

285 to elevated Ca^{2+}/IP_3 levels is insufficient to reduce IP_3 to below 0.5 μM and consequently the transient elevations of Ca^{2+} stops just after 100s followed by a relatively slow degradation of IP_3 and Ca^{2+}: these periodic bursts in Ca^{2+} gives rise to a Ca^{2+} oscillatory wave where the initial Ca^{2+} burst is longer due to synaptic potentiation. At the onset of each subsequent Ca^{2+} burst the IP_3 level drops sharply and we attribute this to strong dependence of IP_3^{3K} on Ca^{2+} (Eq (10)). As the Ca^{2+} level drops J_{chan} (Eq (17))

290 reverses direction perturbing the rate of change in Ca^{2+} (Eq (12)) and this causes a rapid increase in IP_3^{3K} and a corresponding decrease in IP_3 (Eq (11)).

The Ca^{2+} oscillation is initiated at ~20s (T_{CICR} is exceeded; Fig 8) and this triggers the release of glutamate targeting group I mGluRs on the presynaptic terminal, i.e. Glu (e-SP) pathway is activated (Fig 9). Fig 9 shows that the Glu (e-SP) signal accumulates at each CICR and rapidly decays after the Ca^{2+}

295 transients have ceased at ~120 seconds. Also the DSE pathway increases as the activity of the postsynaptic neuron is increasing, and competes with the Glu (e-SP) pathway to restrict PR to a relatively stable low value for all subsequent Ca^{2+} oscillations that occur post-learning, as shown in Fig 10. Again note a longer period of elevation of the DSE signal at the start due to synaptic potentiation but thereafter the DSE profile repeats in time.
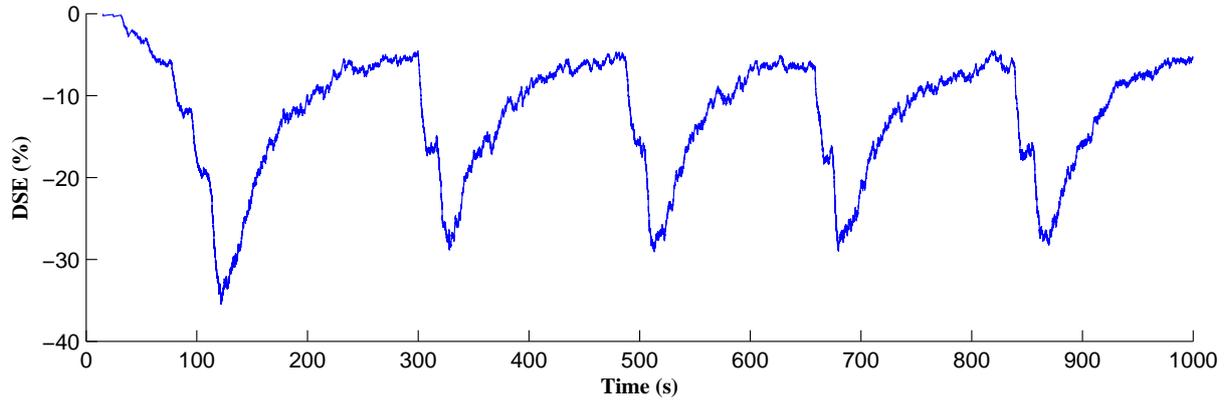
Figure 10. DSE signalling pathway from the postsynaptic neuron, which correlates with the activity of the postsynaptic neuron.
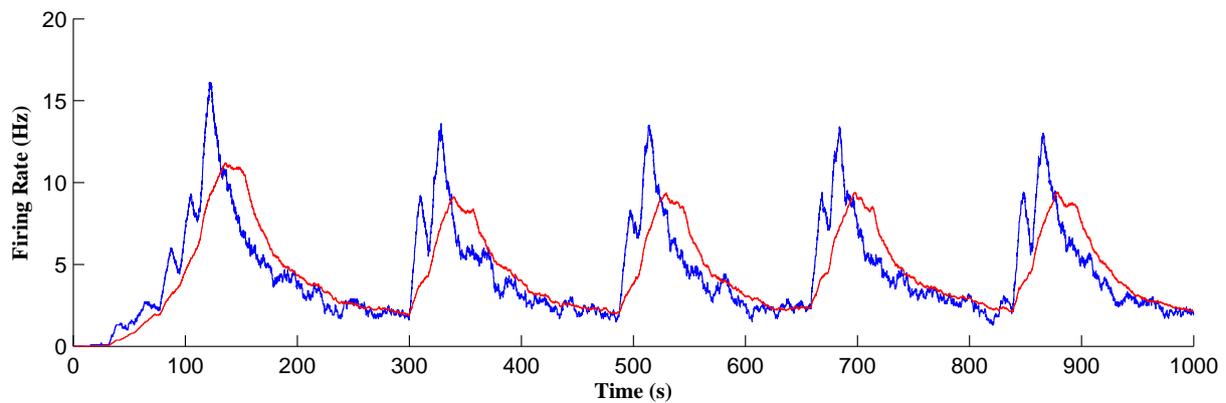
Figure 11. Firing rate of the postsynaptic neuron where a continual bursting behaviour is evident. The firing activity was calculated using a sliding time window of 10 seconds (blue) and again for a sliding window of 40 seconds (red) where the latter gives a better average.

Fig 11 shows the firing rate of the postsynaptic neuron, which is calculated based on a sliding time window of 10 seconds (blue) and 40 seconds (red), respectively. Note that the first burst reaches a higher level of postsynaptic neuron activity when compared to subsequent bursts. Also, between bursts the activity never falls back to zero. This is because the first burst occurs during the weight potentiation phase when the synaptic weight is continually updated and eventually stabilized, whereas in all subsequent neuronal bursts no weight potentiation occurs. Clearly from Fig 11 a continual postsynaptic bursting behaviour is evident.

Referring to Fig 12, we show simulations for f_{pre} of 20Hz, 40Hz and 80Hz where clearly only $f_{pre} = 40Hz$ results in repeated Ca^{2+} oscillations. This is because at 20Hz the T_{CICR} level cannot be reached whereas at 80Hz the astrocyte cytosol is quickly swamped with both IP_3 and Ca^{2+} and subsequent degradation in IP_3 is insufficient to allow further CICR. Consequently our model shows presynaptic frequency selectivity which is consistent with work reported elsewhere (Bienenstock et al., 1982; Dong et al., 2015).

In addition, as the morphology of GABA interneurons and receptor density at the astrocyte cell differ, the IP_3^{GABA} levels vary under the same input f_{pre}. IP_3^{GABA} is a main contributor to the total IP_3, thus the greater IP_3^{GABA}, the longer the process of IP_3 degradation.

Fig 7 shows that when IP_3 degrades sufficiently to once again enable IP_3 to cross T_{CICR} from below, a transient elevation in Ca^{2+} results and PR increases with a corresponding increase in the postsynaptic neuron burst frequency. Therefore, different IP_3^{GABA} levels lead to different burst frequencies of the

postsynaptic neuron. To determine the dependency of neuronal burst frequency on the production rate of IP_3^{GABA}, r_{ip3}^{GABA}, a simulation was carried out (Fig 13) which shows the firing rates of the postsynaptic
320　neuron under different production rates with f_{pre} fixed at 40 Hz. It can be seen that when the r_{ip3}^{GABA}
increases, the frequency of the bursting decreases. For example, for the first 1,000 seconds, there are 6,
5, 4 bursts under the IP_3^{GABA} production rates (r_{ip3}^{GABA}) of 1.8, 2 and 2.2, respectively. This is because
a high IP_3^{GABA} level requires a significant time period to degrade the total IP_3, and to restart the Ca^{2+}
oscillation and bursting behaviour, thus the bursting frequency is low. Note that a fixed frequency of the
325　input stimulus (i.e. f_{pre}=40Hz) is used in this experiment, however the same results are observed for other
f_{pre} values such as 50 Hz, and the burst frequency variation is not constrained for specific f_{pre} values.
The results in Fig 12 and Fig 13 demonstrate the functionalities of the GABA interneuron including the
presynaptic frequency selectivity and postsynaptic bursting frequency regulation.
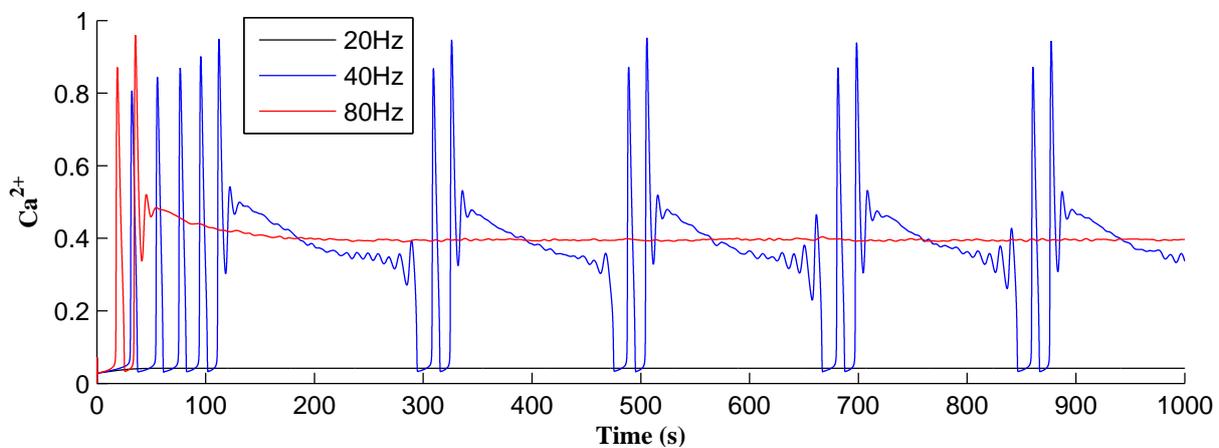
Figure 12. Astrocytic Ca^{2+} as a function of time with f_{pre} of 20, 40 and 80 Hz as a parameter. Note that
for the extreme cases of (20 or 80 Hz) no Ca^{2+} oscillations occur: for f_{pre} = 20 Hz T_{CICR} can never be
achieved and at 80Hz degradation of IP_3 is insufficient to allow CICR to repeatedly occur. Consequently,
there is a frequency window over which oscillations can occur.
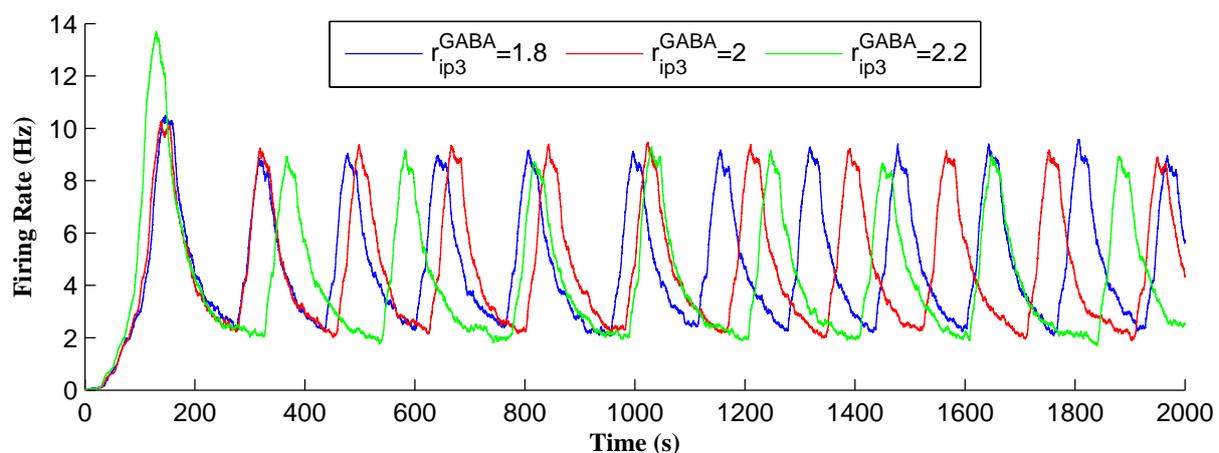
Figure 13. Postsynaptic neuron burst firing as a function of time with IP_3^{GABA} production rates (r_{ip3}^{GABA})
as a parameter. When r_{ip3}^{GABA} increases, IP_3^{GABA} level increases and the frequency of the bursting
decreases. Due to a high IP_3^{GABA} level, a long time period is required to degrade the overall IP_3 and to
restart the Ca^{2+} oscillation. Thus, the bursting frequency is low.

4   CONCLUSIONS

In this paper, a biophysical model is proposed where it is shown that GABA interneuron regulates the astrocytic IP_3 secondary messenger and thus the probability of release (PR) at the presynaptic terminal. In our model we propose that PR modulates the height of the plasticity window and therefore controls when synaptic potentiation/depression occurs. Specifically, the simulations show that during the weight potentiation phase, increasing IP_3 leads to a cycle of CICR events where each is followed by rapid degradation in IP_3. Over time the firing frequency of the postsynaptic neuron continually increases and eventually the synaptic weights stabilise. Postsynaptic firing results in the release of 2-AG into the extracellular space and this messenger binds to CB1R receptors on the astrocyte membrane. The associated IP_3^{AG} contributes to the total cytosolic IP_3 and eventually Ca^{2+} oscillations, and therefore the Glu (e-SP) pathway ceases: 2-AG also binds to CB1Rs on the presynaptic terminal causing a decrease of the synaptic transmission PR via the DSE pathway. PR therefore decreases at the presynaptic terminal which reduces the level of neurotransmitter in the cleft, and consequently the firing frequency of the postsynaptic neuron diminishes, as does IP_3^{AG}. Thereafter, the total IP_3/Ca^{2+} degrades significantly over time but is replenished by IP_3^{GABA} and a subsequent cycle of CICR events commences - the Glu (e-SP) pathway is re-established with an associated increase in PR and the level of neurotransmitter in the cleft is raised. However, in this instance weight potentiation does not occur as $PR < PR^*$. The postsynaptic neuron firing rate increases again until the Ca^{2+} transients stop and thereafter the activity of the postsynaptic neuron falls off again. A network burst has occurred and this is followed by repeated bursts where each coincides with Ca^{2+} transients: the network burst frequency correlates with the Ca^{2+} oscillatory wave. In addition, the GABA released by the GABA interneuron controls the frequency range within which the network bursts can occur. Future work will further explore other neurotransmitters released by astrocytes such as D-serine and ATP, and also slow inward currents at the postsynaptic terminal as a result of glutamate release by astrocytes.

The authors recognize that this study is based on biological findings of the simplest signalling mechanisms involving astrocytic GABA responses and astrocytic glutamate signalling in presynaptic terminals that regulate network function. Other factors, such as astrocytic ATP/adenosine release from astrocytes (Covelo and Araque, 2018), are not considered in the present model, but may also contribute to further shape of network activity, adding further complexity of the network effects of astrocyte signalling. Further studies incorporating these additional elements are therefore required to get a complete view of the astrocyte roles in network function. Despite this the present findings have potential implications for the generation of normal and pathologic circuit behaviour in the brain, relevant to brain diseases that feature altered synaptic properties or where there is a propensity for the episodic synchronised bursting behaviour of neurons. The electroencephalogram (EEG) is a composite product of population-level neuronal firing patterns of differing frequencies. Our findings suggest that GABA-B signalling via astrocytes may be relevant to the generation of certain frequencies and behaviours in the EEG. Seizures are the hallmark of the common brain disease epilepsy and are generated by hyper-synchronous discharges of populations of neurons. Notably, gene expression levels of key components modelled here, including the IP_3 receptor and GABA-B receptor, are dysregulated in human epileptic brain tissue or animal models (Nishimura et al., 2005; Sheilabi et al., 2018; Matsumoto et al., 1996) of epilepsy. Mutations in these genes have also been identified in individuals with epilepsy (Yoo et al., 2017; Møller et al., 2017). Indeed, the GABA-B receptor is a long-standing therapeutic target for the treatment of epilepsy (Bowery, 2006), and more recently the IP_3 receptor was reported to be a target of levetiracetam, one of the most effective anti-epileptic drugs (Nagarkatti et al., 2008). The present model offers a novel mechanism to explain how astrocyte-neuron interactions regulate

seizure-like activity (Gómez-Gonzalo et al., 2010), and how alterations in the described pathways may contribute to hyper-synchronous firing. It may also offer therapeutic insights through targeted manipulation of the astrocytic GABA-B or IP_3 systems followed by evaluation of the resting electroencephalogram (EEG) and investigating whether this alters the frequency or occurrence of pathophysiological neuronal firing and seizures.

CONFLICT OF INTEREST STATEMENT

The authors declare that the research was conducted in the absence of any commercial or financial relationships that could be construed as a potential conflict of interest.

AUTHOR CONTRIBUTIONS

JL, LM, AA, JW, JH, SK, DH, NC, AT, JT, DH investigated and proposed the biophysical model. JL, LM, AA, JW, JH, DH, NC, DH wrote and revised the manuscript. JL, LM, AA, JW, JH, DH, DC, AJ, AT, JT, AM, JH, DH analyzed the results and reviewed the manuscript.

FUNDING

REFERENCES

Alger, B. E. (2002). Retrograde signaling in the regulation of synaptic transmission: Focus on endocannabinoids. *Progress in Neurobiology* 68, 247–286

Araque, A., Parpura, V., Sanzgiri, R. P., and Haydon, P. G. (1999). Tripartite synapses: Glia, the unacknowledged partner. *Trends in Neurosciences* 22, 208–215

Arichi, T., Whitehead, K., Barone, G., Pressler, R., Padormo, F., Edwards, A. D., et al. (2017). Localization of spontaneous bursting neuronal activity in the preterm human brain with simultaneous EEG-fMRI. *eLife* 6, 1–14

Bienenstock, E. L., Cooper, L. N., and Munro, P. W. (1982). Theory for the development of neuron selectivity: Orientation specificity and binocular interaction in visual cortex. *The Journal of Neuroscience* 2, 32–48

Bowery, N. G. (2006). GABAB receptor: A site of therapeutic benefit. *Current Opinion in Pharmacology* 6, 37–43

Breslin, K., Wade, J. J., Wong-Lin, K., Harkin, J., Flanagan, B., Van Zalinge, H., et al. (2018). Potassium and sodium microdomains in thin astroglial processes: A computational model study. *PLoS Computational Biology* 14, 1–25

Covelo, A. and Araque, A. (2018). Neuronal activity determines distinct gliotransmitter release from a single astrocyte. *eLife* 7, 1–19

Dawson, A. P. (1997). Calcium signalling: How do IP3 receptors work? *Current Biology* 7, 544–547

De Pittà, M., Goldberg, M., Volman, V., Berry, H., and Ben-Jacob, E. (2009). Glutamate Regulation of Calcium and IP3 Oscillating and Pulsating Dynamics in Astrocytes. *Journal of Biological Physics* 35, 383–411

Dong, W. S., Zeng, F., Lu, S. H., Liu, A., Li, X. J., and Pan, F. (2015). Frequency-dependent learning achieved using semiconducting polymer/electrolyte composite cells. *Nanoscale* 7, 16880–16889

Flanagan, B., McDaid, L., Wade, J., Wong-Lin, K., and Harkin, J. (2018). A computational study of astrocytic glutamate influence on post-synaptic neuronal excitability. *PLoS Computational Biology* 14, 1–25

410 Foncelle, A., Mendes, A., Jedrzejewska-Szmek, J., Valtcheva, S., Berry, H., Blackwell, K. T., et al. (2018). Modulation of Spike-Timing Dependent Plasticity : Towards the inclusion of a third factor in computational models. *Frontiers in Computational Neuroscience* 12, 1–21. doi:10.3389/fncom.2018. 00049

Gabbiani, F., Metzner, W., Wessel, R., and Koch, C. (1996). From stimulus encoding to feature extraction

415 in weakly electric fish. *Nature* 38, 564–567

Gerstner, W. and Kistler, W. M. (2002). *Spiking neuron models: Single neurons, populations, plasticity* (Cambridge University Press)

Ghosh-dastidar, S. and Adeli, H. (2009). Spiking neural networks. *International Journal of Neural Systems* 19, 295–308

420 Gómez-Gonzalo, M., Losi, G., Chiavegato, A., Zonta, M., Cammarota, M., Brondi, M., et al. (2010). An excitatory loop with astrocytes contributes to drive neurons to seizure threshold. *PLoS Biology* 8, 1–19

Halassa, M. M., Fellin, T., Takano, H., Dong, J., and Haydon, P. G. (2007). Synaptic islands defined by the territory of a single astrocyte. *The Journal of Neuroscience* 27, 6473–6477

Hu, J., Tang, H., Tan, K. C., Li, H., and Shi, L. (2013). A spike-timing-based integrated model for pattern

425 recognition. *Neural computation* 25, 450–72

Izhikevich, E. M. (2003). Simple model of spiking neurons. *IEEE Transactions on Neural Networks* 14, 1569–1572

Johnson, A. P., Liu, J., Millard, A. G., Karim, S., Tyrrell, A. M., Harkin, J., et al. (2018). Homeostatic fault tolerance in spiking neural networks: A dynamic hardware perspective. *IEEE Transactions on Circuits*

430 *and Systems* 65, 687–699

Kullmann, D. M. (2011). Interneuron networks in the hippocampus. *Current Opinion in Neurobiology* 21, 709–716

Kurosinski, P. and Götz, J. (2002). Glial Cells Under Physiologic and Pathologic Conditions. *Archives of Neurology* 59, 1524–1528

435 Li, Y.-X. and Rinzel, J. (1994). Equations for InsP3 receptor-mediated calcium oscillations derived from a detailed kinetic model: A Hodgkin-Huxley like formalism. *Journal of Theoretical Biology* 166, 461–473

Liu, J., Harkin, J., Maguire, L. P., Mcdaid, L. J., and Wade, J. J. (2018). SPANNER: A self-repairing spiking neural network hardware architecture. *IEEE Transactions on Neural Networks and Learning Systems* 29, 1287–1300

440 Liu, J., Harkin, J., McElholm, M., McDaid, L., Jimenez-Fernandez, A., and Linares-Barranco, A. (2015). Case study: Bio-inspired self-adaptive strategy for spike-based PID controller. In *IEEE International Symposium on Circuits and Systems (ISCAS)*. 2700–2703

Liu, J., McDaid, L. J., Harkin, J., Karim, S., Johnson, A. P., Millard, A. G., et al. (2019). Exploring self-repair in a coupled spiking astrocyte neural network. *IEEE Transactions on Neural Networks and*

445 *Learning Systems* 30, 865–875

Lüscher, C. and Malenka, R. C. (2012). NMDA Receptor-Dependent Long-Term Potentiation and Long-Term Depression (LTP/LTD). *Cold Spring Harbor Perspectives in Biology* 4, 1–15

Magee, J. C. and Johnston, D. (1997). A synaptically controlled, associative signal for synaptic plasticity in hippocampal neurons. *Science* 275, 209–213

450 Marchant, J., Callamaras, N., and Parker, I. (1999). Initiation of IP3-mediated Ca2+ waves in Xenopus oocytes. *The EMBO Journal* 18, 5285–5299

Matsumoto, M., Nakagawa, T., Inoue, T., Nagata, E., Tanaka, K., Takano, H., et al. (1996). Ataxia and epileptic seizures in mice lacking type 1 inositol 1,4,5-trisphosphate receptor. *Nature* 379, 168–171

Miles, R. and Wong, R. K. (1986). Excitatory synaptic interactions between CA3 neurones in the guinea pig hippocampus. *The Journal of Physiology* 373, 397–418

Møller, R. S., Wuttke, T. V., Helbig, I., Marini, C., Johannesen, K. M., Brilstra, E. H., et al. (2017). Mutations in GABRB3 From febrile seizures to epileptic encephalopathies. *Neurology* 88, 483–492

Naeem, M., McDaid, L. J., Harkin, J., Wade, J. J., and Marsland, J. (2015). On the role of astroglial syncytia in self-repairing spiking neural networks. *IEEE Transactions on Neural Networks and Learning Systems* 26, 2370–2380

Nagarkatti, N., Deshpande, L. S., and DeLorenzo, R. J. (2008). Levetiracetam inhibits both ryanodine and IP3 receptor activated calcium induced calcium release in hippocampal neurons in culture. *Neuroscience Letters* 436, 289–293

Navarrete, M. and Araque, A. (2010). Endocannabinoids potentiate synaptic transmission through stimulation of astrocytes. *Neuron* 68, 113–126

Nishimura, T., Schwarzer, C., Gasser, E., Kato, N., Vezzani, A., and Sperk, G. (2005). Altered expression of GABA-A and GABA-B receptor subunit mRNAs in the hippocampus after kindling and electrically induced status epilepticus. *Neuroscience* 134, 691–704

Perea, G., Gómez, R., Mederos, S., Covelo, A., Ballesteros, J. J., Schlosser, L., et al. (2016). Activity-dependent switch of GABAergic inhibition into glutamatergic excitation in astrocyte-neuron networks. *eLife* 5, 1–26

Reid, D., Hussain, A. J., and Tawfik, H. (2014). Financial time series prediction using spiking neural networks. *PLoS ONE* 9, 1–13

Serrano, A., Haddjeri, N., Lacaille, J.-c., and Robitaille, R. (2006). GABAergic network activation of glial cells underlies hippocampal heterosynaptic depression. *The Journal of Neuroscience* 26, 5370–5382. doi:10.1523/JNEUROSCI.5255-05.2006

Sheilabi, M. A., Battacharyya, D., Caetano, L., Thom, M., Reuber, M., Duncan, J. S., et al. (2018). Quantitative expression and localization of GABA-B receptor protein subunits in hippocampi from patients with refractory temporal lobe epilepsy. *Neuropharmacology* 136, 117–128

Song, S., Miller, K. D., and Abbott, L. F. (2000). Competitive Hebbian learning through spike-timing-dependent synaptic plasticity. *Nature Neuroscience* 3, 919–926

Wade, J., McDaid, L., Harkin, J., Crunelli, V., and Kelso, S. (2012). Self-repair in a bidirectionally coupled astrocyte-neuron (AN) system based on retrograde signaling. *Frontiers in Computational Neuroscience* 6, 1–12

Wade, J. J., McDaid, L. J., Harkin, J., Crunelli, V., Kelso, J. A. S., and Beiu, V. (2011). Exploring Retrograde Signaling via Astrocytes as a Mechanism for Self Repair. In *International Joint Conference on Neural Networks (IJCNN)* (Ieee), 3149–3155

Yoo, Y., Jung, J., Lee, Y. N., Lee, Y., Cho, H., Na, E., et al. (2017). GABBR2 mutations determine phenotype in rett syndrome and epileptic encephalopathy. *Annals of Neurology* 82, 466–478

APPENDIX

Table 1. GABA interneuron, neuron and synapse parameters.

Parameter	Parameter description	Value	Source
τ_{GABA}	GABA decay rate	10 s	- -
r_{GABA}	GABA production rate	$0.07\ \mu Ms^{-1}$	- -
τ_m	Neuron membrane time constant	24 ms	- -
R_m	Neuron membrane resistance	$1.2G\Omega$	(Wade et al., 2012)
τ_{AG}	2-AG decay rate	10 s	(Wade et al., 2012)
r_{AG}	2-AG production rate	$0.27\ \mu Ms^{-1}$	(Wade et al., 2012)
r_I	Synaptic current production rate	16	- -
PR^*	Learning activation level	0.45	- -
r	Maximum height weighting factor of learning window	40	- -
τ_+	Potentiation width of the plasticity window	40 ms	(Liu et al., 2019)
τ_-	Depression width of the plasticity window	40 ms	(Liu et al., 2019)

Table 2. Astrocyte cell parameters.

Parameter	Parameter description	Value	Source
IP_3^{GABA*}	Baseline value of IP_3^{GABA}	$0.16\ \mu M$	- -
τ_{ip3}^{GABA}	Decay rate of IP_3^{GABA}	7 s	- -
r_{ip3}^{GABA}	Production rate of IP_3^{GABA}	$2\ \mu M$	- -
IP_3^{AG*}	Baseline value of IP_3^{AG}	$0.16\ \mu M$	(Wade et al., 2012)
τ_{ip3}^{AG}	Decay rate of IP_3^{AG}	7 s	(Wade et al., 2012)
r_{ip3}^{AG}	Production rate of IP_3^{AG}	$5\ \mu M$	(Wade et al., 2012)
$K_{PLC\delta}$	Ca^{2+} affinity of PLCδ	$0.1\ \mu M$	(De Pittà et al., 2009)
K_δ	Inhibition constant of PLCδ activity	$1.5\ \mu M$	(De Pittà et al., 2009)
$\bar{r}_{5P}$	IP_3 degradation rate by IP-5P	0.27	- -
$\bar{v}_{3K}$	Maximum degradation rate by IP_3-3K	2	(De Pittà et al., 2009)
K_D	Ca^{2+} affinity of IP_3-3K	0.7	(De Pittà et al., 2009)
K_3	IP_3 affinity of IP_3-3K	1	(De Pittà et al., 2009)
r_C	Maximal CICR rate	$6\ s^{-1}$	(De Pittà et al., 2009)
r_L	Ca^{2+} leakage rate from ER	$0.11\ s^{-1}$	(De Pittà et al., 2009)
v_{ER}	Maximum SERCA pump uptake rate	$0.9\ \mu Ms^{-1}$	(De Pittà et al., 2009)
k_{ER}	SERCA pump activation constant	$0.1\ \mu M$	(De Pittà et al., 2009)
r_{Glu}	Production rate of glutamate	$65\ \mu Ms^{-1}$	- -
τ_{Glu}	Decay rate of glutamate	0.1s	(Wade et al., 2012)
m_{eSP}	e-SP weighting factor	35000	- -
τ_{eSP}	Decay rate of e-SP	40 s	(Wade et al., 2012)
a_2	IP3R Ca^{2+} inactivation binding rate	$0.2\ \mu Ms^{-1}$	(Wade et al., 2012)
c_0	Total free Ca^{2+} cytosol concentration	$2\ \mu M$	(Wade et al., 2012)
c_1	Ratio of ER volume to cytosol volume	0.185	(Wade et al., 2012)
d_1	IP_3 dissociation constant	$0.13\ \mu M$	(Wade et al., 2012)
d_2	Ca^{2+} inactivation dissociation constant	$1.049\ \mu M$	(Wade et al., 2012)
d_3	IP_3 dissociation constant	$0.9434\ \mu M$	(Wade et al., 2012)
d_5	Ca^{2+} activation dissociation constant	$0.08234\ \mu M$	(Wade et al., 2012)
Ca^{2+} threshold	Astrocyte glutamate release Ca^{2+} threshold	$0.7\ \mu M$	- -
K_{AG}	DSE weighting factor	1000	- -